Available online at www.sciencedirect.com
ScienceDirect
International Journal of Machine Tools & Manufacture 46 (2006) 1901–1912
INTERNATIONAL JOURNAL OF MACHINE TOOLS & MANUFACTURE DESIGN, RESEARCH AND APPLICATION
www.elsevier.com/locate/ijmactool

Analytical modeling of spindle–tool dynamics on machine tools using Timoshenko beam model and receptance coupling for the prediction of tool point FRF

A. Ertürk[a], H.N. Özgüven[a], E. Budak[b,*]

[a]Department of Mechanical Engineering, Middle East Technical University, 06531 Ankara, Turkey
[b]Faculty of Engineering and Natural Sciences, Sabanci University, Orhanli, Tuzla, 34956 Istanbul, Turkey

Received 14 December 2005; received in revised form 27 January 2006; accepted 30 January 2006
Available online 3 April 2006

Abstract

Regenerative chatter is a well-known machining problem that results in unstable cutting process, poor surface quality and reduced material removal rate. This undesired self-excited vibration problem is one of the main obstacles in utilizing the total capacity of a machine tool in production. In order to obtain a chatter-free process on a machining center, stability diagrams can be used. Numerically or analytically, constructing the stability lobe diagram for a certain spindle–holder–tool combination implies knowing the system dynamics at the tool tip; i.e., the point frequency response function (FRF) that relates the dynamic displacement and force at that point. This study presents an analytical method that uses Timoshenko beam theory for calculating the tool point FRF of a given combination by using the receptance coupling and structural modification methods. The objective of the study is two fold. Firstly, it is aimed to develop a reliable mathematical model to predict tool point FRF in a machining center so that chatter stability analysis can be done, and secondly to make use of this model in studying the effects of individual bearing and contact parameters on tool point FRF so that better approaches can be found in predicting contact parameters from experimental measurements. The model can also be used to study the effects of several spindle, holder and tool parameters on chatter stability. In this paper, the mathematical model, as well as the details of obtaining the system component (spindle, holder and tool) dynamics and coupling them to obtain the tool point FRF are given. The model suggested is verified by comparing the natural frequencies of an example spindle–holder–tool assembly obtained from the model with those obtained from a finite element software.

Keywords: Chatter stability; Machine tool dynamics; High-performance machining

1. Introduction

Self-excited chatter vibrations caused by regeneration of waviness result in reduced productivity and poor surface finish in machining operations. It is well known that the regeneration effect is related to the phase between two vibration waves during the subsequent cuts on a surface. For certain cutting speeds this phase is minimized increasing stability of the system. Stability diagrams show the stable cutting depths as a function of the cutting speed, and thus can be used to determine stable machining conditions without losing productivity. Therefore, in order to fully employ the capacity of a machine tool under stable cutting conditions it is required to obtain the stability lobe diagram for a certain application using a spindle–holder–tool combination.

History of the stability lobe diagrams and chatter vibrations of machine tools extends to the studies of Tobias [1,3] and Tlusty [2,4] which present the basics of regenerative chatter for orthogonal cutting conditions and time invariant process factors, such as the direction of cutting force and chip thickness. Merrit [5] suggested a theory that uses Nyquist stability criterion yielding similar results for the same conditions. However, the stability analysis of milling is complicated due to the rotational tool resulting in continuously changing directional factors and time-varying system dynamics. The approximate analytical

*Corresponding author. Tel.: +90 216 483 9519; fax: +90 216 483 9550.
E-mail address: ebudak@sabanciuniv.edu (E. Budak).

0890-6955/$ - see front matter © 2006 Elsevier Ltd. All rights reserved.
doi:10.1016/j.ijmachtools.2006.01.032

model for milling stability presented by Tlusty [4] was followed by the time domain simulations [6–8] for prediction of chatter stability in milling. Minis and Yanushevsky [9,10] employed Floquet's theorem and Fourier series for the formulation of milling stability and used Nyquist criterion for the numerical solution. Altintas and Budak [11] presented an analytical milling stability model also by using Floquet's theorem and Fourier series representation of time-varying directional coefficients. They also included the changing dynamics of the machine tool and workpiece in the cutting zone [12]. Regardless of the approach (numerical or analytical), the common point of the models used for generation of stability lobe diagrams is the requirement of the tool point frequency response function (FRF) of the assembly. The well-known relation for the critical width of cut ($b_{\lim}$) for an orthogonal cutting process is given as [13]

$$b_{\lim} = \frac{-1}{2K_f\, m \mathrm{Re}[G(\omega)]}, \tag{1}$$

where K_f is the cutting force coefficient in chip thickness direction, m is the average number of teeth in cut, and $\mathrm{Re}[G(\omega)]$ refers to the real part of the resulting FRF at the cutting point. Thus, the transfer function (in the form of point receptance) $G(\omega)$ is required to obtain the stability lobe diagram of a given spindle–holder–tool combination. Using experimental approach, this FRF can be obtained directly by impact testing. A low-mass accelerometer is placed at the tool tip of the assembly and the system is excited at the same point by using an impulse hammer to obtain the tool point FRF through a spectrum analyzer or modal testing software. However, for a different combination of the system components (even when the overhang length of the tool is changed), a new test will be required since the system dynamics will change. Therefore, the use of experimental modal analysis requires considerable time and therefore is not very practical, as it should be repeated for every holder and tool changes.

In order to minimize experimentation, recently researchers attempted to obtain $G(\omega)$ semi-analytically. Schmitz et al. [14–17] implemented the well known receptance coupling theory of structural dynamics in order to couple the dynamics of the spindle–holder assembly and the tool by using the dynamical properties at the holder–tool interface. Thus, it is suggested to make only a single experiment at the holder tip of the machine tool, and the dynamics of the holder is coupled with the analytically obtained tool dynamics, which is modeled as a uniform Euler–Bernoulli beam, in order to obtain the tool point FRF of the complete system. As long as the dynamical properties at holder–tool interface are analytically modeled or experimentally obtained accurately for different clamping conditions, this semi-analytical model can provide accurate results and may save considerable time in applications where only the conditions related to the cutting tool are changed. It has previously been observed that [18,19] tool overhang length itself is a practical parameter to change the dynamics of the system, especially with its dynamic vibration absorber effect which sometimes makes higher overhang lengths more stable than the lower ones. Schmitz et al. also observed the dynamic absorber effect of tool in their studies [14,15]. Duncan et al. [20] focused on the use of this effect in a recent study.

Several improvements have been done on the receptance coupling approach in the following studies. Park et al. [21] included the rotational degree of freedom at the tool holder–tool joint whereas Kivanc and Budak [22] modeled the tool as a two-segment beam considering the changing area moment of inertia for more accurate results. They also studied the effects of the contact length and the clamping torque on the holder–tool contact stiffness and damping properties. Duncan and Schmitz [23] improved the use of receptance coupling approach to handle different holder types using a single experimental measurement.

Medicus and Schmitz [24] worked on the dynamic repeatability of the tool point FRF for holder and tool changes since repeatability is of quite importance in production applications. As the dynamics of the spindle–holder interface also affects the dynamic stiffness at the tool tip, the literature includes studies that point out the importance of this interface, and suggest alternative connection ways [25–28].

In the study presented here, not only the tool, but all components of spindle–holder–tool assembly are modeled analytically and coupled in order to obtain tool point FRF by using receptance coupling and structural modification methods. The details of the mathematical model are given in this paper. The model developed is used for predicting the tool point FRF of an example spindle–holder–tool assembly and the results are compared with those of a finite element software for verification.

2. Mathematical modeling

2.1. Modeling of component segments

In this study, all components of the spindle–holder–tool assembly are modeled as multi-segment Timoshenko beams. Euler–Bernoulli beam model used in the previous studies [14–17,22,23] has been found to be insufficient for modeling the component dynamics at high frequencies because of their low slenderness ratios since this approach neglects the effects of rotary inertia and shear deformation. In this study, Timoshenko beam model [29,30] is used, and the results are compared with those of Euler–Bernoulli formulation, and a considerable improvement has been observed in the predictions for even relatively slender components.

The eigenvalue problem of an m-segment Timoshenko beam yields a characteristic equation expressed in terms of the determinant of a $4m \times 4m$ matrix. As the elements of the matrix are highly nonlinear, even though the problem and the size of the matrix are physically meaningful, the condition number of such a large order matrix generally

comes out to be very large, which makes it almost impossible to obtain the higher roots of the determinant function accurately. In this study, in order avoid this problem, rather than solving the eigenvalue problems of continuous models of multi-segment beams, only the eigensolution of a uniform, single-segment free–free Timoshenko beam is used. Then, free–free beams of different diameters and lengths are coupled by using their end point FRFs to obtain multi-segment beams representing system components, i.e. spindle, tool holder and tool.

The classical eigensolution of free–free Timoshenko beam is not as simple as that of the Euler–Bernoulli beam. Different approaches, such as numerical, asymptotical and semi-analytical, for the eigensolution of Timoshenko beam, have been suggested in previous works [31–34]. In a more recent study [35] the frequency and mode shape equations of uniform Timoshenko beam with generalized end conditions are presented by using the classical eigensolution. By eliminating some of the terms to obtain free–free end conditions, the characteristic equation can be written as

$$\begin{vmatrix} D_{11} & D_{12} \\ D_{21} & D_{22} \end{vmatrix} = D_{11}D_{22} - D_{12}D_{21} = 0, \tag{2}$$

where

$$D_{11} = (\alpha - \lambda)(\cos\alpha - \cosh\beta), \tag{3}$$

$$D_{12} = (\lambda - \alpha)\sin\alpha + \frac{\lambda\alpha}{\beta\delta}(\beta - \delta)\sinh\beta, \tag{4}$$

$$D_{21} = -\lambda\alpha\sin\alpha + \frac{\alpha - \lambda}{\delta - \beta}\delta\beta\sinh\beta, \tag{5}$$

$$D_{22} = \lambda\alpha(\cosh\beta - \cos\alpha). \tag{6}$$

Here, α and β are the dimensionless frequency numbers given by

$$\alpha = \sqrt{\Omega + \varepsilon}, \quad \beta = \sqrt{-\Omega + \varepsilon}, \tag{7}$$

where

$$\Omega = \frac{b^2(s^2 + R^2)}{2}, \quad \varepsilon = b\sqrt{\frac{1}{4}b^2(s^2 + R^2)^2 - (b^2s^2R^2 - 1)}, \tag{8}$$

$$b^2 = \frac{\rho A\omega^2 L^4}{EI}, \quad s^2 = \frac{EI}{k'AGL^2}, \quad R^2 = \frac{I}{AL^2}. \tag{9}$$

Here, ρ is the density, E is Young's modulus, G is the shear modulus, k' is the shear coefficient, A is the cross-sectional area, I is the cross-sectional area moment of inertia and L is the length of the beam. Note that, for a beam with hollow circular cross-section (which is the general cross-sectional geometry of spindle and holder) the shear coefficient is given as [36]

$$k' = \frac{6(1 + \nu)(1 + m^2)^2}{(7 + 6\nu)(1 + m^2)^2 + (20 + 12\nu)m^2}, \tag{10}$$

where ν is the Poisson's ratio of the beam material and m is the inner to outer diameter ratio of the cross-section ($m = d_{\text{inner}}/d_{\text{outer}}$). For a circular cross-section which is not hollow (such as that of a cutting tool) $d_{\text{inner}} = 0$ and the expression for the shear coefficient becomes

$$k' = \frac{6(1 + \nu)}{7 + 6\nu}. \tag{11}$$

From the reduced frequency equation of free–free Timoshenko beam (Eq. (2)), the natural frequency of the r-th elastic mode can be obtained, and the dimensionless frequency numbers α_r and β_r of that mode can be calculated. By using these values, the eigenfunction expressions can be obtained as

$$\phi_r(x) = A_r\Big[C_1\sin\Big(\frac{\alpha_r}{L}x\Big) + C_2\cos\Big(\frac{\alpha_r}{L}x\Big) + C_3\sinh\Big(\frac{\beta_r}{L}x\Big) + C_4\cosh\Big(\frac{\beta_r}{L}x\Big)\Big] \tag{12}$$

for the dynamic transverse deflection of the beam, and as

$$\psi_r(x) = \frac{A_r}{L}\Big[\lambda_r\Big(C_1\cos\Big(\frac{\alpha_r}{L}x\Big) - C_2\sin\Big(\frac{\alpha_r}{L}x\Big)\Big) + \delta_r\Big(C_3\cosh\Big(\frac{\beta_r}{L}x\Big) + C_4\sinh\Big(\frac{\beta_r}{L}x\Big)\Big)\Big] \tag{13}$$

for the dynamic bending rotation. Here

$$\lambda_r = \alpha_r - \frac{b^2s^2}{\alpha_r}, \quad \delta_r = \beta_r + \frac{b^2s^2}{\beta_r}, \tag{14}$$

$$C_1 = L, \quad C_2 = -\frac{D_{11}}{D_{12}}C_1, \quad C_3 = \frac{\alpha_r - \lambda_r}{\delta_r - \beta_r}C_1,$$
$$C_4 = -\frac{\lambda_r}{\beta_r}\frac{\alpha_r}{\delta_r}\frac{D_{11}}{D_{12}}C_1 \quad (r = 1, 2, 3, \ldots), \tag{15}$$

and A_r is a constant obtained by the mass normalization of the eigenfunctions such that the following orthogonality condition is satisfied:

$$\int_{x=1}^{x=L}\{U_r(x)\}^T[M]\{U_s(x)\}\,dx = \begin{cases} 1, r = s \\ 0, r \neq s \end{cases} \tag{16}$$

where

$$\{U_r(x)\} = \begin{Bmatrix} \phi_r(x) \\ \psi_r(x) \end{Bmatrix}, \quad [M] = \begin{bmatrix} \rho A & 0 \\ 0 & \rho I \end{bmatrix}. \tag{17}$$

Note that, due to the existence of shear distortion, the bending slope function $\psi_r(x)$ is not equal to the derivative of the lateral deflection function $\phi_r(x)$. Since the beam has free end conditions, there also exist two rigid body modes with the mass-normalized eigenfunctions

$$\phi_0^{\text{trans}}(x) = \sqrt{\frac{1}{\rho AL}}, \tag{18}$$

$$\phi_0^{\text{rot}}(x) = \sqrt{\frac{12}{\rho AL^3}}\Big(x - \frac{L}{2}\Big). \tag{19}$$

$\phi_0^{\text{trans}}(x)$ and $\phi_0^{\text{rot}}(x)$ represent the translational and rotational rigid body eigenfunctions, respectively.

Let the end points of the beam be denoted by numbers 1 and 2 as shown in Fig. 1. Using the mass-normalized eigenfunctions, one might find all the receptance functions that relate the linear and angular displacements to the forces and the moments applied at these points. The receptance functions are denoted by letters H, N, L and P and they are defined as follows:

$$\begin{aligned} y_j &= H_{jk} f_k, \quad \theta_j = N_{jk} f_k, \\ y_j &= L_{jk} m_k, \quad \theta_j = P_{jk} m_k, \end{aligned} \tag{20}$$

where y and θ represent the linear and angular displacements, respectively, and f and m are the forces and the moments, respectively, applied at the points of interest (j and k, which take the values of 1 and 2 in this case).

By assuming structural damping with a loss factor of γ, the receptances defined above can be expressed as a function of excitation frequency ω as

$$H_{jk} = \sum_{r=0}^{\infty} \frac{\phi_r(x_j)\,\phi_r(x_k)}{(1+\mathrm{i}\gamma)\omega_r^2 - \omega^2}, \tag{21}$$

$$N_{jk} = \sum_{r=0}^{\infty} \frac{\phi_r'(x_j)\,\phi_r(x_k)}{(1+\mathrm{i}\gamma)\omega_r^2 - \omega^2}, \tag{22}$$

$$L_{jk} = \sum_{r=0}^{\infty} \frac{\phi_r(x_j)\,\phi_r'(x_k)}{(1+\mathrm{i}\gamma)\omega_r^2 - \omega^2}, \tag{23}$$

$$P_{jk} = \sum_{r=0}^{\infty} \frac{\phi_r'(x_j)\,\phi_r'(x_k)}{(1+\mathrm{i}\gamma)\omega_r^2 - \omega^2}, \tag{24}$$

where $j = 1, 2$ and $k = 1, 2$. In Eqs. (21)–(24), i is the unit imaginary number and $\phi_r'(x)$ is the derivative of $\phi_r(x)$ with respect to x.

By substituting Eqs. (12), (18) and (19) into Eqs. (21)–(24), the point and transfer FRFs of points 1 and 2 can be obtained. For instance, the direct FRFs of point 1 (for $j = 1$ and $k = 1$) will take the following form

$$H_{11} = \frac{-1}{\rho A L \omega^2} + \frac{-3}{\rho A L \omega^2} + \sum_{r=1}^{\infty} \frac{\phi_r(L)\,\phi_r(L)}{(1+\mathrm{i}\gamma)\omega_r^2 - \omega^2}, \tag{25}$$

$$N_{11} = \frac{-6}{\rho A L^2 \omega^2} + \sum_{r=1}^{\infty} \frac{\phi_r'(L)\,\phi_r(L)}{(1+\mathrm{i}\gamma)\omega_r^2 - \omega^2}, \tag{26}$$

$$L_{11} = \frac{-6}{\rho A L^2 \omega^2} + \sum_{r=1}^{\infty} \frac{\phi_r(L)\,\phi_r'(L)}{(1+\mathrm{i}\gamma)\omega_r^2 - \omega^2}, \tag{27}$$

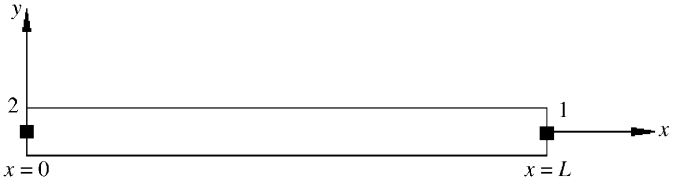

Fig. 1. Uniform Timoshenko beam with free end conditions.

$$P_{11} = \frac{-12}{\rho A L^3 \omega^2} + \sum_{r=1}^{\infty} \frac{\phi_r'(L)\,\phi_r'(L)}{(1+\mathrm{i}\gamma)\omega_r^2 - \omega^2}. \tag{28}$$

The remaining 12 FRFs of the beam can be obtained in a similar manner.

Having obtained all the end point FRFs of a single-segment beam by using sufficient number of modes in the summation term for each segment, one might now couple required number of free–free beams to form the desired multi-segment beam and find its end point FRFs, as explained in the following section.

2.2. Coupling of component segments

Consider Fig. 2a in which two single-segment Timoshenko beams with free end conditions are coupled to represent a two-segment free–free beam. The receptance matrices of the free–free beams A and B can be written as

$$[A] = \begin{bmatrix} [A_{11}] & [A_{12}] \\ [A_{21}] & [A_{22}] \end{bmatrix}, \tag{29}$$

$$[B] = \begin{bmatrix} [B_{11}] & [B_{12}] \\ [B_{21}] & [B_{22}] \end{bmatrix}, \tag{30}$$

where each submatrix includes the point and transfer receptance functions of the segment end points. For example, the point receptance matrix of point $A1$ in beam A is given as

$$[A_{11}] = \begin{bmatrix} H_{A1A1} & L_{A1A1} \\ N_{A1A1} & P_{A1A1} \end{bmatrix}. \tag{31}$$

Note that $[A_{11}]$ actually represents $[A_{A1A1}]$, and just for simplicity it is depicted as $[A_{11}]$ in this paper (the same is true

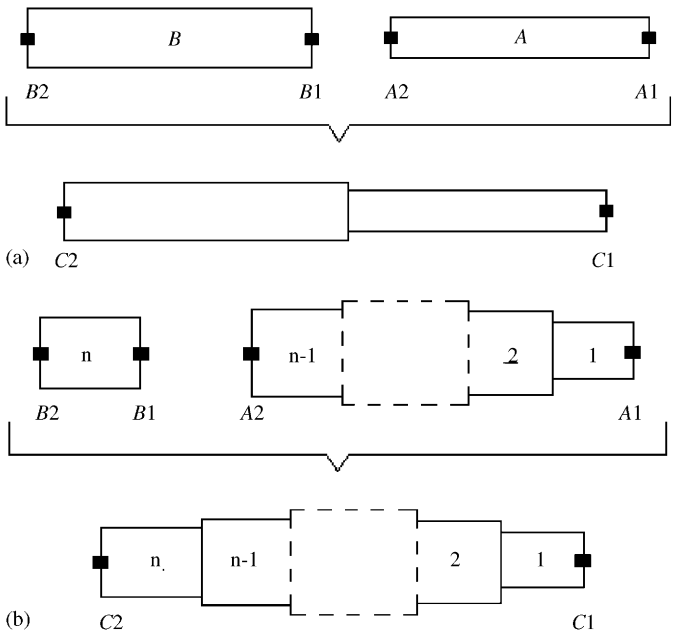

Fig. 2. (a) Rigid coupling of two uniform beams with free end conditions and (b) rigid coupling of the n-th segment.

for other similar submatrices). Similarly, the other point and transfer receptance matrices can be expressed for segments A and B.

After writing the individual displacement–force (and moment) relations for beams A and B, and expressing the compatibility and continuity relations at the connection point, one can obtain the receptance matrix of the two-segment beam C as

$$[C] = \begin{bmatrix} [C_{11}] & [C_{12}] \\ [C_{21}] & [C_{22}] \end{bmatrix}, \tag{32}$$

where

$$[C_{11}] = [A_{11}] - [A_{12}][[A_{22}] + [B_{11}]]^{-1}[A_{21}], \tag{33}$$

$$[C_{12}] = [A_{12}][[A_{22}] + [B_{11}]]^{-1}[B_{12}], \tag{34}$$

$$[C_{21}] = [B_{21}][[A_{22}] + [B_{11}]]^{-1}[A_{21}], \tag{35}$$

$$[C_{22}] = [B_{22}] - [B_{21}][[A_{22}] + [B_{11}]]^{-1}[B_{12}]. \tag{36}$$

It is also possible to couple the dynamics of two segments by impedance coupling [37]. Impedance coupling has the general advantage of calculating the receptances of internal points as well, at the expense of increased matrix sizes. However, in our case, we only need the tool point receptance, and therefore the receptance coupling approach is more advantageous as it reduces the computational effort. Furthermore, as far as condition numbers of resulting matrices are considered, it is obviously preferable to deal with matrices of lower dimensions. In a very similar way, one might continue coupling more segments like a chain to form an n-segment beam with the same boundary conditions as illustrated in Fig. 2b.

By bringing beams of different diameters and lengths together, the receptance matrices of main components of the system, i.e. spindle, holder and tool, can be calculated. Obviously, the multi-segment components built this way will have free–free boundary conditions. However, spindle, which is one of the main components, is supported by bearings. This implies adding dynamics of the bearings to the spindle at the bearing locations as springs and dampers. In this study, the dynamics of the bearings are included to the system by using structural modification approach.

2.3. Including bearing dynamics

As the receptance coupling method used in this study allows the computation of end point receptances only, the effect of bearing dynamics is to be included into the system dynamics while coupling the segment where bearing is connected. Then, it can be coupled to the rest of the system. For instance, let us consider the spindle given in Fig. 3. If we start from the right end, the two segments on the right-hand side of the bearing can be coupled rigidly to form a two-segment free–free beam, and then bearing dynamics is added to the left end of this two-segment beam as shown in Fig. 4. Note that, when the bearing is not connected to the end point

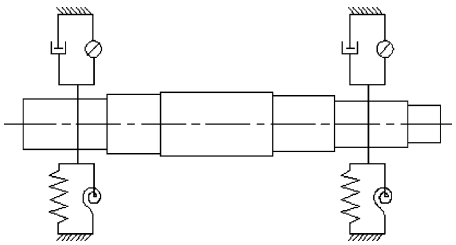

Fig. 3. Simple spindle model: multi-segment beam grounded by springs and dampers.

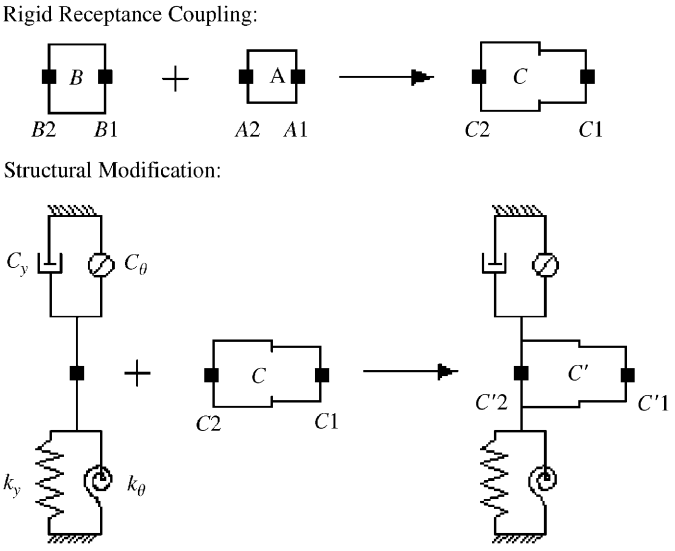

Fig. 4. Receptance coupling of two segments and addition of bearing dynamics to the system by structural modification.

of a uniform segment, the uniform segment where the bearing is connected must be represented by two parts. As a consequence, in the example system shown in Fig. 3, we have eight effective segments although it is a six-segment beam. The structural modification method of Özgüven [38] is used in including bearing stiffness and damping into system dynamics. In this method, the receptance matrix of unmodified system and the properties of the modifications are used to calculate the receptance matrix of the modified system. First, the receptance matrices of segments A and B are coupled as given by Eqs. (33)–(36) and the receptance matrix of the two-segment beam C is obtained as follows:

$$[C] = \begin{bmatrix} H_{C1C1} & L_{C1C1} & H_{C1C2} & L_{C1C2} \\ N_{C1C1} & P_{C1C1} & N_{C1C2} & P_{C1C2} \\ H_{C2C1} & L_{C2C1} & H_{C2C2} & L_{C2C2} \\ N_{C2C1} & P_{C2C1} & N_{C2C2} & P_{C2C2} \end{bmatrix}. \tag{37}$$

For the structural modification formulation, the receptance matrix given by Eq. (37) should be rearranged as

$$[\alpha_C] = \begin{bmatrix} H_{C1C1} & H_{C1C2} & L_{C1C1} & L_{C1C2} \\ H_{C2C1} & H_{C2C2} & L_{C2C1} & L_{C2C2} \\ N_{C1C1} & N_{C1C2} & P_{C1C1} & P_{C1C2} \\ N_{C2C1} & N_{C2C2} & P_{C2C1} & P_{C2C2} \end{bmatrix}. \tag{38}$$

Let $[D]$ be the dynamic structural modification matrix which includes the translational and rotational, stiffness and damping information of the bearing:

$$[D] = \begin{bmatrix} 0 & 0 & 0 & 0 \\ 0 & K_y & 0 & 0 \\ 0 & 0 & 0 & 0 \\ 0 & 0 & 0 & K_\theta \end{bmatrix}, \tag{39}$$

where

$$K_y = k_y + \mathrm{i}\omega c_y, \tag{40}$$

$$K_\theta = k_\theta + \mathrm{i}\omega c_\theta, \tag{41}$$

and they are the translational and rotational complex stiffness expressions, respectively, representing the stiffness and damping of the bearing. However, it should be noted that, spindle bearings can be represented by translational stiffness only as usually self-aligning types are used and they do not carry moment. When this is the case, K_θ is taken to be zero in the above equation. Then, the receptance matrix of the modified system (C') can be obtained from

$$[\alpha_{C'}] = [[I] + [\alpha_C]\,[D]]^{-1}\,[\alpha_C], \tag{42}$$

which can be written in terms of partitioned matrices [38] as

$$\left[\alpha_{C'}^{11}\right] = \left[[I] + \left[\alpha_C^{11}\right]\,[D^{11}]\right]^{-1}\,\left[\alpha_C^{11}\right], \tag{43}$$

$$\left[\alpha_{C'}^{12}\right]^{\mathrm{T}} = \left[\alpha_{C'}^{21}\right] = \left[\alpha_C^{21}\right]\,\left[[I] - [D^{11}]\,\left[\alpha_{C'}^{11}\right]\right], \tag{44}$$

$$\left[\alpha_{C'}^{22}\right] = \left[\alpha_C^{22}\right] - \left[\alpha_C^{21}\right]\,\left[D^{11}\right]\,\left[\alpha_{C'}^{12}\right]. \tag{45}$$

Here $[I]$ is the identity matrix and $[D^{11}]$ is the sub-matrix of the structural modification matrix $[D]$ when its elements are rearranged yielding

$$[D] = \begin{bmatrix} [D^{11}] & [0] \\ [0] & [0] \end{bmatrix}, \tag{46}$$

where

$$\left[D^{11}\right] = \begin{bmatrix} K_y & 0 \\ 0 & K_\theta \end{bmatrix}. \tag{47}$$

Note that, rearranging the modification matrix implies arranging the unmodified receptance matrix given by Eq. (38), as well. As can be seen from Eqs (43)–(45), such an arrangement of the elements of Eq. (38) reduces the order of the matrices in operation from 4 to 2. As a result, when this approach (Ref. [38]) is used, only a single matrix of order two is to be inverted. Further efficiency in calculations can be obtained by using an effective algorithm [39].

After the structural modification due to the first bearing is made, the dynamics of the other segments can be included by applying the receptance coupling procedure repeatedly until the section where the next bearing is connected. Then, a similar structural modification is applied in order to include the dynamics of the other bearing. Finally, the other segments of the spindle are coupled to the rest of the system to obtain the end point receptance matrices for the complete spindle.

2.4. Coupling of components

After the end point receptances for each component (spindle, holder and tool) are obtained, a similar receptance coupling procedure can be employed to find the receptances of the coupled system as shown in Fig. 5a. However, in dynamic coupling of components, the contact stiffness and damping representing the joint between these components have to be considered as well. Therefore, the receptance coupling formulation for the dynamic coupling of components will be slightly different from the above formulation given for the coupling of segments.

Note that in Fig. 5a each component is modeled as a multi-segment beam. Since the holder is usually tapered, in this study it is modeled using uniform beams of different diameters. In order to form the assembly seen in Fig. 5a, the receptance matrices of the components will be coupled elastically. Fig. 5b shows the components to be joined in order to form the spindle–holder–tool assembly. As can be seen in Fig. 5b, the part of the holder inside the spindle is considered as integrated to the spindle; and similarly, the part of the tool inside the holder is considered as rigidly joined to the holder. Such an approach provides a more realistic model, as otherwise only the dynamics due to the masses of these parts will be included into the model or it will be required to include their stiffness effects with distributed springs. Then, two of the above components

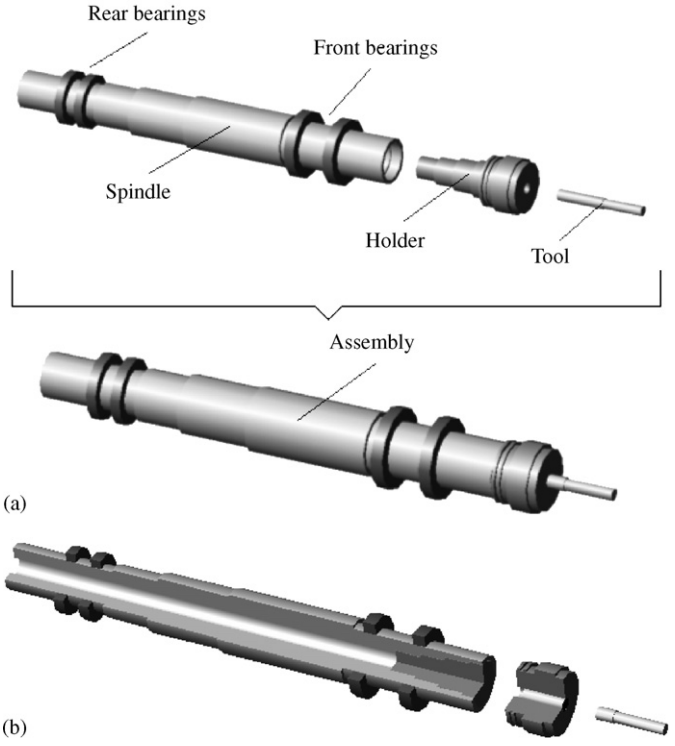

Fig. 5. (a) Components of a spindle-holder-tool system and their combination and (b) components to be coupled elastically (sectional view).

will have composite segments. However, note that, the contact stiffness and damping parameters representing the spindle–holder and holder–tool connections should be determined by considering the actual geometry.

Fig. 6 summarizes the elastic coupling of spindle, holder and tool. Here, $[K_{sh}]$ is the complex stiffness matrix representing spindle-holder interface dynamics:

$$[K_{sh}] = \begin{bmatrix} k_y^{sh} + i\omega c_y^{sh} & 0 \\ 0 & k_\theta^{sh} + i\omega c_\theta^{sh} \end{bmatrix}, \quad (48)$$

where k_y^{sh} is the translational stiffness, c_y^{sh} is the translational damping, k_θ^{sh} is the rotational stiffness and c_θ^{sh} is the rotational damping at the spindle–holder interface. After obtaining the end point receptance matrices of subsystem S (spindle on bearings) and subsystem H (holder), the end point FRFs of the combined system SH (spindle + holder) can be obtained by receptance coupling as explained in Section 2.2. However, in this case, the receptance matrices of components are coupled through elastic elements, and therefore the resulting equations will be slightly different from those given by Eqs. (33)–(36):

$$[SH_{11}] = [H_{11}] - [H_{12}]\left[[H_{22}] + [K_{sh}]^{-1} + [S_{11}]\right]^{-1}[H_{21}], \quad (49)$$

$$[SH_{12}] = [H_{12}]\left[[H_{22}] + [K_{sh}]^{-1} + [S_{11}]\right]^{-1}[S_{12}], \quad (50)$$

$$[SH_{21}] = [S_{21}]\left[[H_{22}] + [K_{sh}]^{-1} + [S_{11}]\right]^{-1}[H_{21}], \quad (51)$$

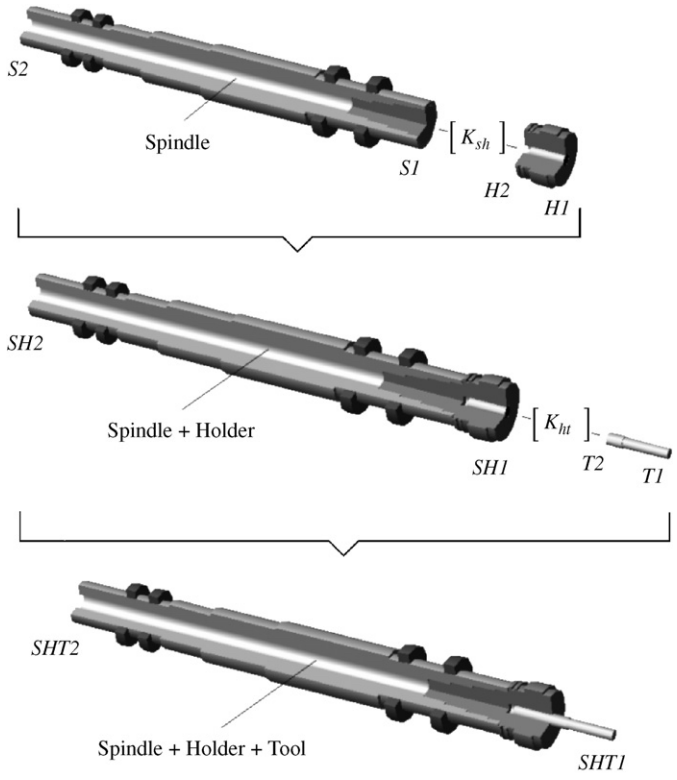

Fig. 6. Elastic coupling of spindle, holder and tool (sectional view).

$$[SH_{22}] = [S_{22}] - [S_{21}]\left[[H_{22}] + [K_{sh}]^{-1} + [S_{11}]\right]^{-1}[S_{12}]. \quad (52)$$

Similarly, the receptance matrix of the tool can be coupled with the rest of the system as depicted Fig. 6, and the resulting matrices of the final assembly (spindle, holder and tool) can be obtained in a very similar manner. The FRF required to construct the stability lobe diagram of a given spindle–holder–tool combination is the one which provides the relation between the transverse displacement and the force at the tip of the tool, which is the direct point FRF at the tool tip. It is the first element of the point FRF matrix of the tool tip which can be obtained as

$$[SHT_{11}] = [T_{11}] - [T_{12}]\left[[T_{22}] + [K_{ht}]^{-1} + [SH_{11}]\right]^{-1}[T_{21}], \quad (53)$$

where subsystem T represents the tool and $[K_{ht}]$ is the complex stiffness matrix of the holder–tool interface dynamics as shown in Fig. 6.

$$[K_{ht}] = \begin{bmatrix} k_y^{ht} + i\omega c_y^{ht} & 0 \\ 0 & k_\theta^{ht} + i\omega c_\theta^{ht} \end{bmatrix}. \quad (54)$$

Here, k_y^{ht} is the translational stiffness, c_y^{ht} is the translational damping, k_θ^{ht} is the rotational stiffness and c_θ^{ht} is the rotational damping at the holder–tool interface. Note that elastic impedance coupling can be considered as an alternative to elastic receptance coupling [37]. As mentioned earlier, impedance coupling reduces the number of calculation steps at the cost of dealing with matrices of higher dimensions and reduced computational efficiency due to storing the dynamic information of unnecessary points.

3. Case study and discussion of results

In this section, the model developed is used to calculate the point receptance function at the tool tip of a typical spindle–holder–tool assembly analytically. It is also aimed to validate the mathematical model by comparing the natural frequencies with those obtained from a finite element model of the system. The numerical results and the computational efficiency of the model are also discussed.

3.1. Prediction of tool point FRF

The geometry of the spindle–holder–tool combination used in the case study is shown in Fig. 7, and the dimensions of the components, bearing and interface dynamical properties of the assembly are given in Tables 1–3. The material is steel with mass density $\rho = 7800\,kg/m^3$, Young's modulus $E = 200\,GPa$ and Poisson's ratio $\nu = 0.3$. In addition, the material loss factor is assumed to be $\gamma = 0.003$. Typical values from the literature are used for bearing and interface dynamics. Numerical values identified in a recent study [40] are used for bearing and

spindle–holder interface dynamics, and for the holder–tool interface dynamics, the values given in Refs. [14,15] are used. Since the contact damping values do not affect the natural frequencies of the resulting tool point FRF, very light damping is used for the bearings and the interfaces. The magnitude and phase diagrams of the tool point FRF obtained by using the model developed in this study are shown in Fig. 8. The tool point FRF $G(\omega)$ found from the model can now directly be used in the analytical model presented by Budak et al. [11] to obtain the stability lobe diagram of the spindle–holder–tool combination in order to determine the spindle speed–axial depth of cut combinations for stable machining.

At this point, it is worthwhile to mention the importance of using Timoshenko beam theory rather than Euler–Bernoulli beam model. It is very well known that rotary inertia and especially shear deformation [41] are very important for non-slender components and/or at high frequencies. In order to demonstrate the effect of using Timoshenko beam theory, two example FRF plots from the intermediate steps of the case study are given. The first one (Fig. 9) is the point FRF at the tip of the spindle before it is connected to the holder and the tool, and the second one (Fig. 10) is the point FRF of the free–free tool (excluding the part inside the holder) before it is joined to the system. Note that, the maximum percentage error in natural frequencies within the frequency ranges of Figs. 9 and 10, due to using Euler–Bernoulli model, is 15% for the spindle and 19% for the tool. Based on these results, it can be concluded that Euler–Bernoulli model may yield inaccurate results (especially at high frequencies) when it is used in this analytical model as well as in similar semi-analytical models (such as classical tool coupling). However, when the resulting tool point FRFs obtained for both models are considered (Fig. 11) it can be seen that the results of both models are fairly in agreement for the same frequency range of Fig. 8.

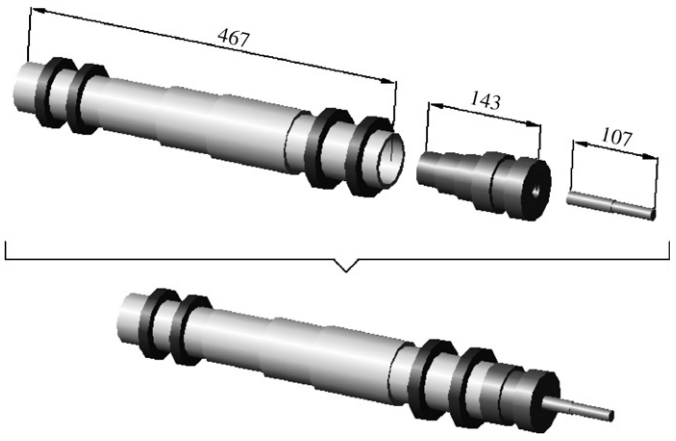

Fig. 7. Components of the case study and their assembly.

Table 2
Average dynamical properties of the bearings and interfaces

	Translational stiffness (N/m)	Rotational stiffness (N m/rad)
Front bearings (for each)	7.5×10^5	—
Rear bearings (for each)	2.5×10^6	—
Spindle–holder interface	5×10^7	1.5×10^6
Holder–tool interface	2×10^7	1.5×10^6

Table 3
Distances of the bearings measured from the right end of the spindle

Bearing no.[a]	Bearing 1	Bearing 2	Bearing 3	Bearing 4
Distance (mm)	26	78	387	427

[a]The bearings are measured from the right end of the spindle and numbered starting from the same point.

Table 1
Component dimensions:[a] (a) spindle; (b) holder; and (c) tool

(a) *Spindle dimensions*

Segment number	1	2	3	4	5	6	7	8	9	10
Length (mm)	26	26	26	38	100	66	75	30	40	40
Outer diameter (mm)	66	66	66	66	76	70	62	58	58	58
Inner diameter (mm)	54	48	40	32	32	32	32	32	32	32

(b) *Holder dimensions*

Segment number	1	2	3	4	5	6
Length (mm)	22	19	24	26	26	26
Outer diameter (mm)	72	60	70	54	48	40
Inner diameter (mm)	16	16	16	16	16	16

(c) *Tool dimensions*[b]

Segment number	1	2
Length (mm)	50	57
Outer diameter (mm)	14	16
Inner diameter (mm)	0	0

[a]Component segments are numbered starting from the right end of their given figures.
[b]The overhang length of the tool is 85 mm for the given combination.

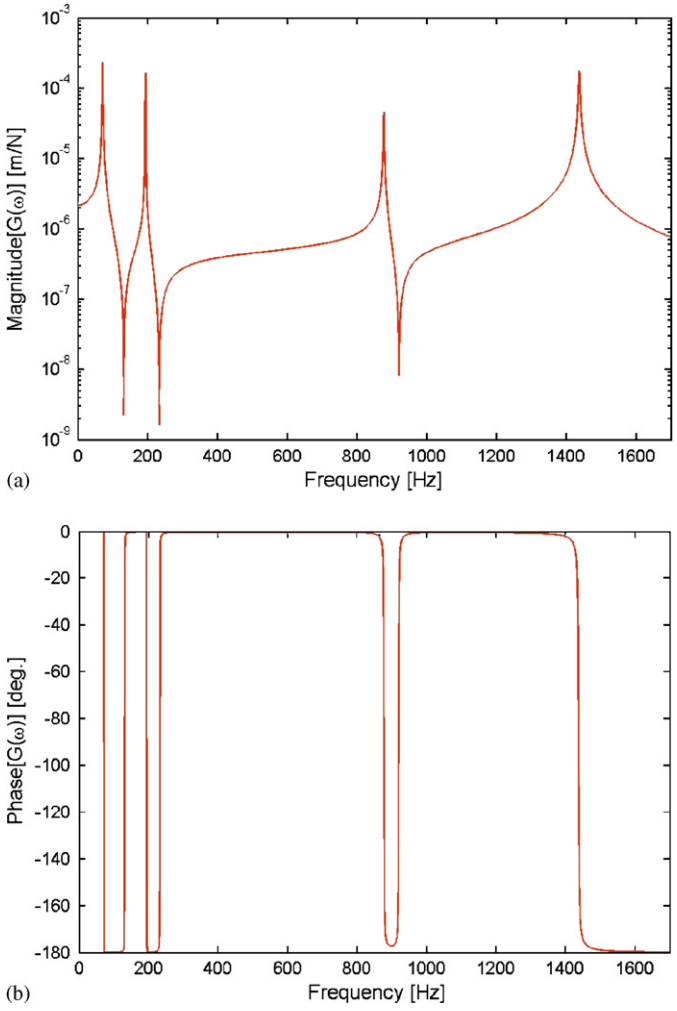

Fig. 8. Tool point FRF $G(\omega)$ of the assembly: (a) magnitude diagram and (b) phase diagram.

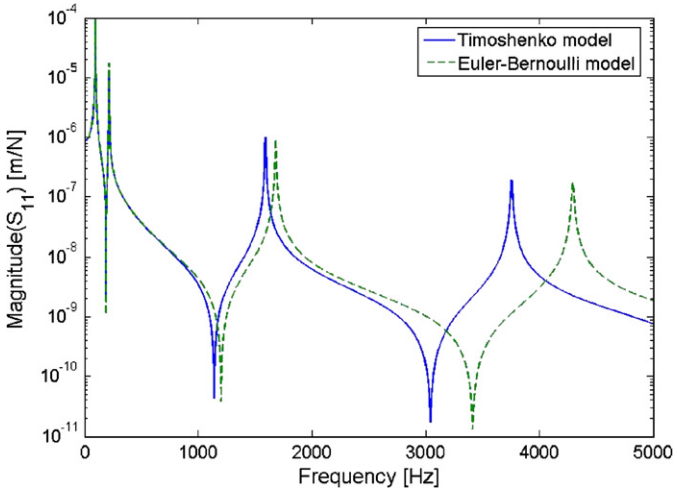

Fig. 9. Point FRF at the spindle tip (the holder and tool are not connected).

Note that, in Fig. 8, the material loss factor is taken to be very small in order to observe the peaks better; especially, the peak of the fifth mode which tends to disappear for

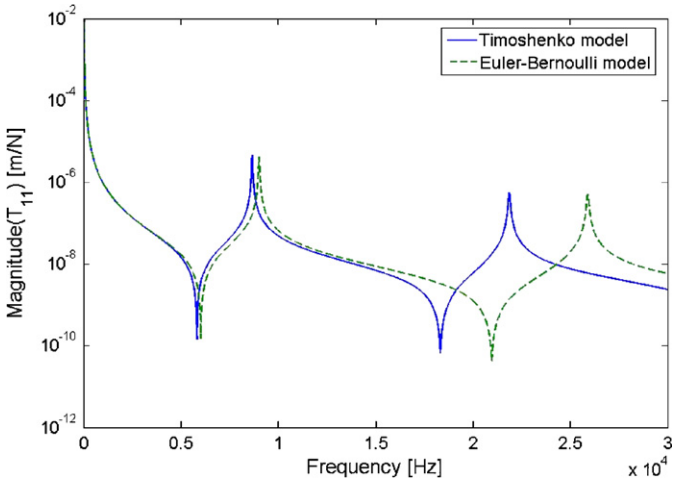

Fig. 10. Point FRF of the free–free tool (excluding the part inside the holder).

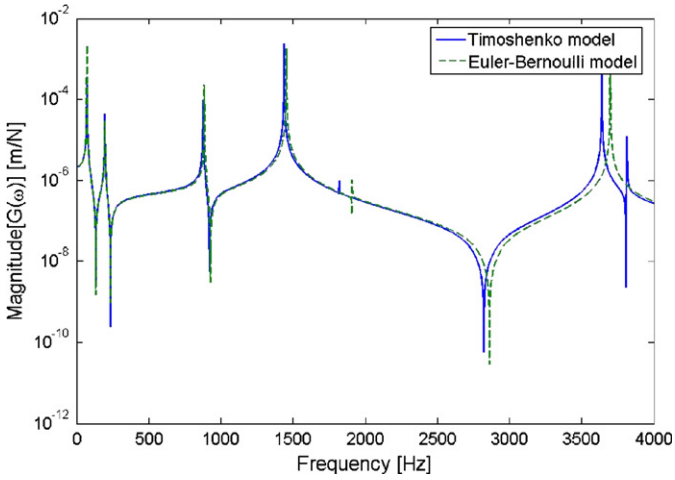

Fig. 11. Tool point FRF for the example case (material loss factor is taken as close to zero).

even light material damping. This agreement is due to the fact that at lower frequencies the FRFs are primarily controlled by the elasticity of the interfaces between spindle–holder and holder–tool, rather than the flexural rigidities of the holder and tool themselves. In the frequency range of interest, the part of the holder outside the spindle behaves almost as a mass with no elastic contribution, and the elastic contribution of the tool is at most from its first mode. As can be seen in Fig. 11, an additional mode comes into the picture in Timoshenko model, which is not captured by Euler–Bernoulli model at relatively high frequencies (around 3800 Hz in this case). It can be concluded that, in case of stiffer connection dynamics (so that component structural behaviors become more important) and/or when the frequency range of interest is wider (and consequently higher modes are of interest), it becomes a must to use Timoshenko model for accurate results. Deficiency of Euler–Bernoulli model in

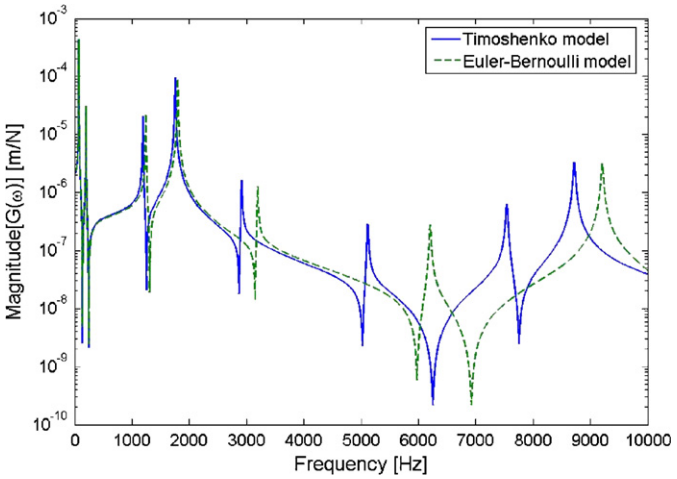

Fig. 12. Tool point FRF for highly stiff connection at spindle–holder and holder–tool interfaces.

such a case is illustrated in Fig. 12 which shows the tool point FRF of the same assembly when a much stiffer connection is assumed between the components and the frequency range is extended to 10000 Hz.

In the previous studies that use Euler–Bernoulli model with classical tool receptance coupling, good agreements between experimental and predicted FRFs were obtained. However, it should be noted that in these studies the connection parameters at the holder–tool interface were obtained by fitting the model to the experiment tool point FRFs. In such an approach, depending on the component geometries, i.e. slenderness ratios, and connection dynamics, using Euler–Bernoulli beam theory rather than Timoshenko beam theory may result in modeling errors which can be compensated by the incorrect connection parameters identified, and consequently the experimental and predicted FRFs are expected to be in agreement. However, then both free tool FRFs and connection parameters would be in error. Consequently, it can be said that Euler–Bernoulli beam theory can be used only for lower frequencies and/or with high slenderness, and furthermore if our interest is only the tool point FRF, not those of individual components. Still extreme care is to be taken.

3.2. Finite element model results

In order to verify the results of the model suggested in this paper, the assembly of the case study (Fig. 7) is modeled using a reliable finite element software, ANSYS® 9.0. Beam element BEAM188 of the software, which is based on Timoshenko beam theory is used for modeling the components. Even though these two-node beam elements used for constructing the components are capable of handling six degrees of freedom at each node, the degrees of freedom other than motion in one transverse direction and flexural rotation are restricted so that the finite element model is consistent with the model proposed in this paper and no additional irrelevant modes (such as axial or torsional vibration modes) come into the picture. In order to represent the dynamics of bearings and spindle–holder and holder–tool interfaces, combination element COMBIN14 (Spring-Damper) of ANSYS® 9.0 is used.

Table 4
Natural frequencies of the assembly used in the case study

	Model (Hz)	ANSYS® 9.0 (Hz)	Difference (%)
Mode 1	71.7	71.6	0.14
Mode 2	195	193.8	0.62
Mode 3	877.8	867.5	1.19
Mode 4	1438.3	1424.3	0.98
Mode 5	1819.5	1752.6	3.82
Mode 6	3639.3	3442.5	5.72
Mode 7	3812.5	3634.8	4.89

The natural frequencies of the assembly obtained by the analytical model proposed and the finite element model constructed in ANSYS® 9.0 are tabulated in Table 4. The percentage difference between the model and FEA predictions are also shown in Table 4. As can be seen from the table, the natural frequencies of the assembly obtained by the model presented in this paper and those obtained by using the finite element software are in good agreement and the maximum difference observed for the first seven modes is about 5%.

The FRF analysis of the assembly is performed in ANSYS® 9.0 and the tool point FRF (for the frequency range of 0–1700 Hz with a frequency increment of 0.5 Hz) is obtained in 45 min on a workstation (2 × Intel® Xeon 2.00 GHz CPU, 1.00 GB RAM). The same FRF is obtained by the analytical model proposed (for the same frequency range and frequency increment) in less than a minute on a PC (1 × Intel® Centrino 1.70 GHz CPU, 256 MB RAM), which indicates a considerable decrease in computational time (more than 45 times faster for the case study), in addition to the saving in preparing input data (due to avoiding time required for modeling and meshing operations in FEA).

4. Conclusions

In this paper, an analytical method that uses receptance coupling and structural modification techniques is presented for modeling spindle–holder–tool assemblies in machining centers in order to obtain the tool point FRF which is required for prediction of chatter stability. The resulting FRF can directly be used in existing numerical or analytical models to construct the stability lobe diagram of the assembly.

The results of the model are compared with those obtained by using finite element software ANSYS® 9.0 for verification. It is observed that the natural frequencies

obtained by the model proposed and by the finite element software are in good agreement. It is also observed that, using the model proposed for obtaining the tool point FRF reduces the computational time considerably (by a factor of 45 in the case study presented) compared with using FE analysis. That the model does not require complicated modeling and meshing operations in computer environment is also another advantage which makes it simpler and less expensive than FE analysis.

As the components involved (spindle, holder and tool) are not slender enough to neglect the effects of shear deformation and rotary inertia, Timoshenko beam theory is used for modeling their dynamics. The assembly used in the case study is also modeled by using Euler–Bernoulli beam theory in order to observe possible differences from the Timoshenko beam theory results. From the observations made in Section 3, it is concluded that the beam theory used may not be so crucial at low-frequency region where the vibrations are primarily controlled by the elasticity of the connection points rather than component flexural rigidities. However, it is observed that Euler–Bernoulli model may yield inaccurate results at high frequencies and/or for stiffer connection dynamics. It is also concluded that if the individual component FRFs are of interest, it becomes a must to use Timoshenko beam theory since the structural dynamics will be the only source of vibrations.

The model can be used in predicting and following the changes in the tool point FRF due to possible variations in tool and holder types and/or tool length very quickly and in a very practical way. Although it is possible to use a finite element model for a spindle-holder–tool assembly for the same purpose, it will always be more costly both in constructing the model and in the computation time as demonstrated with a numerical example. Furthermore, it will not be practical to use a finite element model in studies requiring repeated dynamic analyses with several different geometries and/or configurations, as it is the case in design of spindles. At the stage of spindle design, for instance, the model can be used in order to obtain the maximum dynamic stiffness at the spindle tip at a required frequency. Thus, lengths, inner and outer diameters of the segments, as well as the bearing locations and preloads (therefore the stiffnesses) can be varied in order to optimize the spindle geometry at a required frequency (or frequency range). Since the analytical model suggested in this paper is very efficient, especially compared with the finite element models, various design alternatives can easily be tried and numerical results can be obtained in a very short time with a minimum effort.

Acknowledgments

This project is funded by the Scientific and Technological Research Council of Turkey (TUBITAK) under Project number 104M430 which is gratefully acknowledged.

References

[1] S.A. Tobias, W. Fishwick, The chatter of lathe tools under orthogonal cutting conditions, Transactions of ASME 80 (1958) 1079–1088.
[2] J. Tlusty, M. Polacek, The stability of machine tools against self-excited vibrations in machining, in: Proceedings of the ASME International Research in Production Engineering, Pttsburgh, USA, 1963, pp. 465–474.
[3] S.A. Tobias, Machine Tool Vibration, Blackie and Sons Ltd., London, 1965.
[4] F. Koenisberger, J. Tlusty, Machine Tool Structures—vol.I: Stability Against Chatter, Pergamon Press, Englewood Cliffs, NJ, 1967.
[5] H. Merrit, Theory of self-excited machine tool chatter, Transactions of ASME Journal of Engineering for Industry 87 (1965) 447–454.
[6] J. Tlusty, F. Ismail, Basic nonlinearity in machining chatter, Annals of the CIRP 30 (1981) 21–25.
[7] J. Tlusty, Dynamics of high-speed milling, Transactions of ASME Journal of Engineering for Industry 108 (2) (1986) 59–67.
[8] S. Smith, J. Tlusty, Efficient simulation programs for chatter in milling, Annals of the CIRP 42 (1) (1993) 463–466.
[9] I. Minis, T. Yanushevsky, R. Tembo, R. Hocken, Anaylsis of linear and nonlinear chatter in milling, Annals of the CIRP 39 (1990) 459–462.
[10] I. Minis, T. Yanushevsky, A new theoretical approach for prediction of machine tool chatter in milling, ASME Journal of Engineering for Industry 115 (1993) 1–8.
[11] Y. Altintas, E. Budak, Analytical prediction of stability lobes in milling, Annals of the CIRP 44 (1995) 357–362.
[12] E. Budak, Y. Altintas, Analytical prediction of chatter stability in milling—Part I: general formulation; Part II: application to common milling systems, Transactions of ASME, Journal of Dynamic Systems, Measurement, and Control 120 (1998) 22–36.
[13] J. Tlusty, Manufacturing Processes and Equipment, Prentice Hall, Upper Saddle River, NJ, 2000.
[14] T. Schmitz, R. Donaldson, Predicting high-speed machining dynamics by substructure analysis, Annals of the CIRP 49 (1) (2000) 303–308.
[15] T. Schmitz, M. Davies, M. Kennedy, Tool point frequency response prediction for high-speed machining by RCSA, Journal of Manufacturing Science and Engineering 123 (2001) 700–707.
[16] T. Schmitz, M. Davies, K. Medicus, J. Synder, Improving high-speed machining material removal rates by rapid dynamic analysis, Annals of the CIRP 50 (1) (2001) 263–268.
[17] T. Schmitz, T. Burns, Receptance coupling for high-speed machining dynamics prediction, in: Proceedings of the 21st International Modal Analysis Conference, 3–6 February 2003, Kissimmee, FL (on CD).
[18] M. Davies, B. Dutterer, J. Pratt, A. Schaut, On the dynamics of high-speed milling with long, slender endmills, Annals of the CIRP 47 (1) (1998) 55–60.
[19] S. Smith, W. Winfough, J. Halley, The effect of tool length on stable metal removal rate in high-speed milling, Annals of the CIRP 47 (1) (1998) 307–310.
[20] G.S. Duncan, M.F. Tummond, T.L. Schmitz, An investigation of the dynamic absorber effect in high-speed machining, International Journal of Machine Tools and Manufacture 45 (2005) 497–507.
[21] S.S. Park, Y. Altintas, M. Movahhedy, Receptance coupling for end mills, International Journal of Machine Tools and Manufacture 43 (2003) 889–896.
[22] E.B. Kivanc, E. Budak, Structural modeling of end mills for form error and stability analysis, International Journal of Machine Tools and Manufacture 44 (2004) 1151–1161.
[23] G.S. Duncan, T. Schmitz, An improved RCSA model for tool point frequency response prediction, in: Proceedings of the 23rd International Modal Analysis Conference, 30 January–3 February 2005, Orlando, FL (on CD).

[24] K. Medicus, T. Schmitz, Evaluating the tool point dynamic repeatability for high-speed machining applications, in: Proceedings of the 16th Annual ASPE Meeting, 11–15 November 2001, Arlington, VA, pp. 357–360.
[25] E. Rivin, Influence of toolholder interfaces on tooling performance, Transactions of NAMRI/SME (1993) 173–179.
[26] M. Weck, I. Schubert, New interface machine/tool: hollow shank, Annals of the CIRP 43 (1) (1994) 345–348.
[27] J. Agapiou, E. Rivin, C. Xie, Toolholder/spindle interfaces for CNC machine tools, Annals of the CIRP 44 (1) (1995) 383–387.
[28] S. Smith, T.P. Jacobs, J. Halley, The effect of drawbar force on metal removal rate in milling, Annals of the CIRP 48 (1) (1999) 293–296.
[29] S.P. Timoshenko, On the correction for shear of the differential equation for transverse vibrations of prismatic bars, Philosophical Magazine 41 (1921) 744–746.
[30] S.P. Timoshenko, On the transverse vibrations of bars of uniform cross-section, Philosophical Magazine 43 (1922) 125–131.
[31] P.A.A. Laura, R.H. Gutierrez, Analysis of vibrating Timoshenko beams using the method of differential quadrature, Shock and Vibration 1 (1) (1993) 89–93.
[32] S.M. Han, H.B. Benaroya, T. Wei, Dynamics of transversely vibrating beams using four engineering theories, Journal of Sound and Vibration 225 (5) (1999) 935–988.
[33] B. Geist, J.R. McLaughlin, Asymptotic formulas for the eigenvalues of the Timoshenko beam, Journal of Mathematical Analysis and Applications 253 (2001) 341–380.
[34] J. Lee, W.W. Schultz, Eigenvalue analysis of Timoshenko beams and axisymmetric Mindlin plates by the pseudospectral method, Journal of Sound and Vibration 269 (2004) 609–621.
[35] J.D. Aristizabal-Ochoa, Timoshenko beam-column with generalized end conditions and nonclassical modes of vibration of shear beams, Journal of Engineering Mechanics 130 (10) (2004) 1151–1159.
[36] R. Blevins, Formulas for Natural Frequency and Mode Shape, Van Nostrand Reinhold Co., NY, 1979.
[37] A. Ertürk, E. Budak, H.N. Özgüven, Dynamic modeling of spindle–tool holder–tool assembly in machining centers, in: Proceedings of 12th National Symposium on Theory of Machines, 9–11 June 2005, Kayseri, Turkey, vol.I, pp. 15–26 (in Turkish).
[38] H.N. Özgüven, Structural modifications using frequency response functions, Mechanical Systems and Signal Processing 4 (1) (1990) 53–63.
[39] H.N. Özgüven, A new method for harmonic response of non-proportionally damped structures using undamped modal data, Journal of Sound and Vibration 117 (1987) 313–328.
[40] N. Arakere, T. Schmitz, C. Cheng, Rotor dynamic response of a high-speed machine tool spindle, in: Proceedings of the 23rd International Modal Analysis Conference, 30 January–3 February 2005, Orlando, FL (on CD).
[41] W. Weaver, S.P. Timoshenko, D.H. Young, Vibration Problems in Engineering, Wiley Interscience, NY, 1990.